Cattelan, M., Vagin, M. Y., Fox, N., Ivanov, I. G., Shtepliuk, I., & Yakimova, R. (2019). Anodization study of epitaxial graphene: insights on the oxygen evolution reaction of graphitic materials. *Nanotechnology*, *30*(28), [285701]. https://doi.org/10.1088/1361-6528/ab1297

University of Bristol - Explore Bristol Research
General rights

Anodization study of epitaxial graphene: insights on the oxygen evolution reaction of graphitic materials.

Anodization study of epitaxial graphene: insights on the oxygen evolution reaction of graphitic materials.

Mattia Cattelan[1], Mikhail Yu. Vagin[2,3], Neil A. Fox[1], Ivan G. Ivanov[2], Ivan Shtepliuk[2], Rositsa Yakimova [2]

[1] School of Chemistry, University of Bristol, Cantocks Close, Bristol BS8 1TS, UK.

[2] Department of Physics, Chemistry and Biology, Linköping University, SE-581 83, Linköping, Sweden.

[3] Laboratory of Organic Electronics, Department of Science and Technology, Linköping University, SE-601 74, Norrköping, Sweden.

E-mail: Dr. Mattia Cattelan mattia.cattelan@bristol.ac.uk

Abstract

The photoemission electron microscopy and x-ray photoemission spectroscopy were utilized for the study of anodized epitaxial graphene on silicon carbide as a fundamental aspect of the oxygen evolution reaction on graphitic materials. The high-resolution analysis of surface morphology and composition quantified the material transformation during the anodization. We investigated the surface with lateral resolution <150 nm, revealing significant transformations on the epitaxial graphene and the role of multilayer edges in increasing the film capacitance.

Supplementary material for this article is available online

1. Introduction

Graphene, graphite and carbon nanotubes belong to the family of graphitic materials based on a framework of sp^2 carbon atoms, and they are employed for several applications in different research and industrial fields that involve catalysis [1-6]. In this context they are either used as a conductive support for a series of catalytic materials [7] or as metal-free active compounds [1, 8, 9]. The production of graphitic materials can be achieved by various methods such as chemical vapour deposition, exfoliation and thermal annealing [10, 11]. The latter is used to grow high-quality graphene layers on silicon carbide substrates which are referred as to Epitaxial Graphene (EG) because the layers are azimuthally-ordered with respect to the substrate lattice [12]. EG exhibits exceptional electronic and structural properties and have been studied by several surface science techniques [12, 13].

In this work electrochemical processing has been conducted on EG. This approach is quite unusual [14, 15] because typically the electrochemical studies are made on bulk graphitic materials, e.g. multilayer graphene oxide, using large surface areas to maximize the active sites [16-21]. Unfortunately, such preparation methods induce a variety of defects and functionalities that are difficult to control [16] and make it problematic to identify the active electrochemical sites. Using EG for the electrochemical study solves this problem due to the relatively low-defect density of the surface.

Moreover, advanced surface analytical tools, such as Photo Emission Electron Microscopy (PEEM) and X-ray Photoelectron Spectroscopy (XPS), can be employed to investigate in detail the surface chemical and physical transformations due to the electrochemical treatments.

Electrochemistry is also a powerful method to modify material properties. For example, it is well-known that graphitic materials are oxidation resistant and particularly strong conditions must be employed to produce defects on the basal planes [22-24]. In this work EG has been selectively anodized and oxygen-functionalized to shed light on its possible use as an Oxygen Evolution Reaction (OER) catalyst. Indeed, this chemical reaction has been studied using graphitic materials either as a metal-free catalyst, such as with carbon nanotubes [19] and C-N composites, or as a support for active species [25, 26], however it is still not clear how the carbon sp^2 framework behaves and modifies during the reaction.

Therefore, we decided to anodize EG layers, as EG is an ideal ultra-thin graphitic material and the anodization is a fundamental aspect of the OER. We analysed the samples by photoemission techniques, such as PEEM and XPS. UltraViolet-PEEM is sensitive to only few surface atoms and it is rarely employed for electrochemical studies but owing to the use of this technique we were able to study with unprecedented lateral resolution (<150 nm) the anodization effects on the surface.

We performed PEEM and XPS for different degrees of anodization to understand the material changes. With the combination of both macro- and microscopic chemical data we obtained information about the mechanism of graphene fragmentation, diffusion pathways of oxygen moieties, the behaviour of multilayers and gas evolution effects. The surface analyses have been acquired on samples at different anodization stages. The very distinct sample conditions from wet electrochemistry to Ultra-High Vaccum (UHV) made it impratical to perform our measurements on the same sample for different anodization times, as has been performed in previous literature works using solid electrolytes [27-29]. All of this information is crucial to the future use of carbon sp^2 materials for OER.

2. Experimental section

2.1 Samples and processes

An Autolab type III potentiostat (Autolab, EcoChemie, Netherlands) was used for the electrochemical measurements. An Ag/AgCl electrode in 3 M KCl and a platinum wire were used as reference electrode and counter electrode, respectively, for all measurements.

The samples of nominally monolayer EG on SiC (substrate area 7×7 mm² and thickness 0.4 mm) and the electrochemical cell employed for the measurements have been obtained from Graphensic AB. Graphene was grown on the Si-face of the SiC substrates which typically yields a continuous coverage of more than 90% of monolayer graphene while the remainder is small patches of bilayer graphene [30].

The monolayer and multilayer regions of EG on the sample were distinguished using reflectance mapping [31], and an example is shown in Supplementary Data Figure S3. The sample contains a high percentage of monolayer graphene (~ 98 %) decorated with miniature islands of bilayer graphene which cover ~ 2 % of the surface. The laser power incident on the sample was ~17 mW when focused to a spot with a diameter of approximately 0.85 μm.

The electrochemical cell consisted of a 300 μl cup with a 2 mm diameter hole sealed with a Viton O-ring disk on the bottom. The EG sample was fixed under the hole with the O-ring using screws on the lid. A dry contact to the EG was formed by an aluminum adhesive. The mounted sample was kept inside the cell during all electrochemical measurements in order to avoid sample drift.

The EG electrode anodization was carried out in a 0.1 M KNO_3 solution in a continuous pulsed mode with a 0.5 second oxidation pulse at 2 V followed by a 0.125 second reduction pulse at 0.1 V [14].

The OER study was performed by voltammetry in 1 M NaOH.

2.2 Photoemission studies

Photoemission studies were carried out at the Bristol NanoESCA facility, in two connected UHV chambers with a base pressure of 2×10^{-11} mbar. XPS was acquired with Al Kα (1486.7 eV) monochromatic in a spot of few mm. The pass energy was set 50 eV for survey spectra and 6 eV for High Resolution (HR) data. Total energy resolution was about 300 meV for the HR data.

PEEM Work Function (WF) measurements were acquired close to the WF threshold with a non-monochromatic Hg lamp (≈5.2 eV). The pass energy was set to 50 eV and slit 0.5 mm obtaining a total energy resolution of 140 meV. The lateral resolution of the maps was better than 150 nm. The WF maps have been obtained by fitting with a "complementary error function", the stack of snapshots at different E-E$_F$ values around the WF threshold at every pixel location in each snapshot image. The WF values have been corrected for the Schottky effect due to the high extractor field, ΔE =98 meV for 12 kV with a sample distance of 1.8 mm.[32]

3. Results and discussion

3.1 Electrochemical measurements

The impedance spectra acquired for pristine and anodized EG samples in an aqueous electrolyte showed a well-defined semi-circle in a complex plane plot of the frequency-normalized admittance (Figure 1, Table 1) from which the

Table 1. The values of coverage calculated from reflectivity, electrical double layer capacitance estimated on different samples. Relative difference of capacitance has been calculated by averaging the capacitance calculated by the fitting by Circle (C) and Equivalent Circuit (EC).

Sample	Mono-, bilayer, %	Condition	Fitting Method, Circle (C) or Equivalent Circuit (EC)	Specific capacitance, ($\mu F \ast cm^{-2}$)	Capacitance relative difference after anodization ($\Delta - \Delta \, pristine$)/$\Delta \, pristine$
Pristine	98.0 ~1.9	Pristine	C	15.61	/
Anodized #1	97.5 2.5	Pristine	C	11.46	0.42
		Anodized, 30 s	C	15.61	
			EC*	16.88	
Anodized #2	96.5 3.5	Pristine	C	14.33	0.59
		Anodized, 430 s	C	23.25	
			EC*	22.29	

*See Supporting Note 1 in Supplementary Data.

electrical double layer capacitance on the EG surface can be visualized.

The spectra obtained for the longer period of anodization were analyzed also with equivalent circuits [14] in order to take into account more complex impedance patterns. For the anodized samples, the variation in double layer capacitance estimated for pristine samples revealed an inverse correlation with the monolayer content (Figure S4), which can illustrate the increased contribution from the edges of the multilayers at high capacitance; evidence of this phenomenon is reported below in section 3.3 and 3.4.
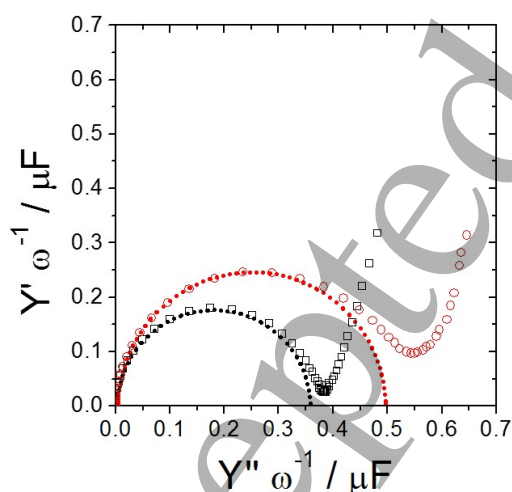

Figure 1. The increase of double layer capacitance by anodization. Impedance spectra in complex capacitance coordinates obtained for pristine (□) and anodized for 30 seconds EG (O; 0.1 M KNO₃, 0 V, 50 kHz – 1 Hz, 5 mV amplitude); dashed curves represent spectra fitted with circle.

The anodization led to an expected increase of capacitance due to both the fracturing of the EG layer yielding the

formation of reactive defect sites, [14, 33] and the removal of contaminants from the EG surface. The relative change of the electrical double layer capacitance by anodization showed an inverse correlation with the monolayer content and non-monotonic evolution with increasing anodization time, which probably illustrates the complex contribution from multi-layered EG remaining unaffected by treatment [14].

The anodization process was investigated by voltammetry in alkaline media. The high anodic polarization displayed the appearance of an oxidative process illustrating the OER on EG, as shown in Figure 2. Importantly, the appearance of visible currents occurred at significant overpotential of ca. 1.4 V, which is much higher than those reported for other OER catalysts [34]. The electrode sustained only a small current density of OER of 0.3 mA cm^{-2} visualized by the maintenance of current density on repeated cycle. The higher current density of 1.2 mA cm^{-2} reached by the increase in anodic polarization led to graphene degradation, as evidenced by the decrease in the currents on repeated cycles. The Tafel slope of observed OER on graphene was 120 mV decade^{-1}, which is reported for a variety of mechanistic models of OER [34, 35]. Higher current densities revealed the appearance of smaller Tafel slope (90 mV decade^{-1}). The peculiar decrease of Tafel slope with the current density increase shows the change of the rate-determining step of the process, which, probably, manifests in the graphene degradation that is observed.
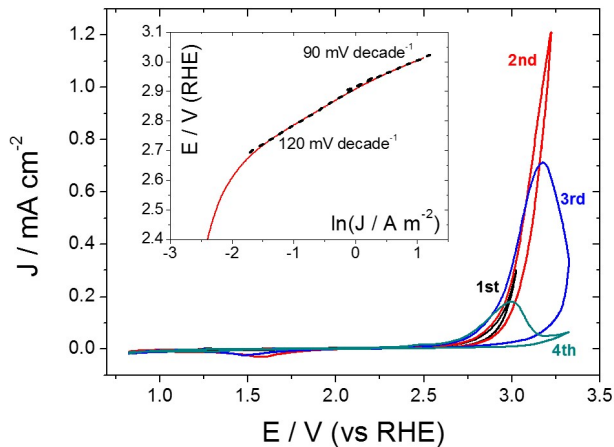
Author *et al*

Figure 2. Anodization due to OER on epitaxial graphene. The cyclic voltammograms were acquired on EG electrode with anodic limit increase (1M NaOH, 20 mV s⁻¹). Inset: the IR-compensated polarization curve derived from the first voltammetry cycle in Tafel plot.

3.2 XPS measurements

The samples were annealed under UHV conditions before acquiring XPS and WF maps, to desorb from the surface the adsorbed water and contaminants arising from the air exposure. This preparation step is necessary because of the extreme surface sensitivity of the PEEM acquisitions (few surface atoms). XPS surveys indicated that the only species present on the samples' surfaces were oxygen, carbon and silicon demonstrating their cleanliness after the electrochemical treatment. It is well-know that annealing in a reducing atmosphere can modify oxygen-functionalized graphene [36]. To avoid not modifying the oxygen functionalities on the anodized layers, step annealing from 100 °C to 500 °C in steps of 50 °C were carried out on a strongly anodized sample and the chemical composition of the surface was studied by XPS at each step. Heating up the sample to more than 250 °C resulted in a decrease in the oxygen functionalities of the layer, which is a result consistent with the reduction under UHV of graphene oxide samples [37]. The anodized samples #1 and #2 were subsequently heated up to 150 °C for 45 minutes before the PEEM analysis, whereas the pristine sample had been heated up to 275 °C to remove as much of the contaminants as possible.

Presented in Figure 3 are the XPS spectra of Carbon 1*s* photoemission lines, for the pristine sample and the two anodized samples. We have tentatively deconvoluted the C 1*s* photoemission lines into single chemically shifted components. For the pristine sample three main components at 283.8, 285.0 and 286.0 eV are present which correspond to carbon in SiC, carbon in graphene and multilayer graphene and carbon in the buffer layer respectively [38]. In the pristine sample, signals of C and Si bonded with oxygen are missing, indeed, the O photoemission line for this sample is barely detectable and this may be related to some macro impurities on the sample.
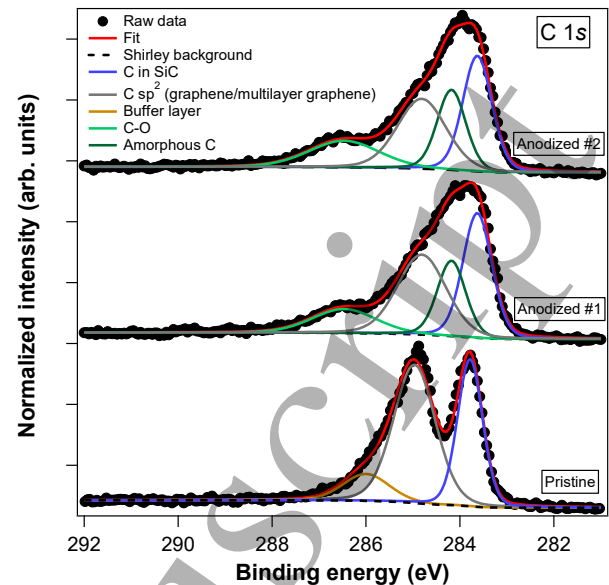

Figure 3. Normalized XPS C 1*s* photoemission lines for pristine and anodized samples #1 and #2. The photoemission lines are deconvoluted in single chemically shifted components. The red, black dashed line are for the total fit and the Shirley background respectively. The raw data are represented by black circles marks. The purple, grey, orange, light green and dark green are for C in SiC, C hybridized sp², C in buffer layer, C single bonded with oxygen and amorphous C respectively.

After the anodization the Si 2*p* (Figure S5) and C 1*s* photoemission lines shift towards low Binding Energies (BEs). We hypothesized that this phenomenon can be associated with the decoupling of the graphene layer from the SiC substrate and therefore a change of band bending due to a modification of interfacial charges. This shift has been observed for the intercalation of hydrogen [39] water [40] and oxygen [41] for graphene on SiC. In our experiment, the shift of the photoemission lines is about 0.16 eV, which is lower than the one measured for graphene on SiC decoupled with oxygen [41]. However, the process reported here is complex; the films undergo both a physical and chemical transformation, as is made visible by the WF maps reported later, and in contrast to previous work where intercalating agents were presumed to only saturate the dangling bonds of the substrate. Indeed, we do not observe a rigid shift of the lines [39-41] but a deep transformation of the spectra. We therefore decided to attempt a careful deconvolution into single chemically shifted components of the C 1*s* photoemission lines.

To perform a consistent fitting the spectra of C 1*s*, Si 2*p* and O 1*s* they have been normalized by the total area of C 1*s*. The anodized samples have very similar oxygen contents (Figure S5) even if #2 has been electrochemically processed for a longer time. This phenomenon can be due to the continuous redistribution of oxygen moieties on the surface, see discussion in section 3.4. The difference between the
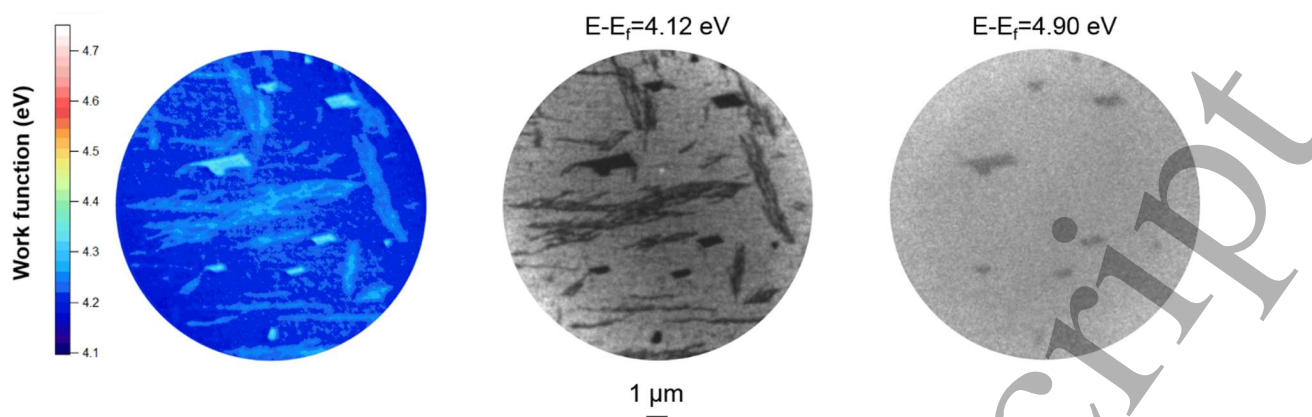
Figure 4. EG PEEM analysis. On the left the WF map on the centre and right the snapshots acquired at E-E_F= 4.12 and 4.90 eV.

anodized samples #1 and #2 is made clearer by noting the decrease of the Si 2p lines (Figure S3), which can be explained by the dramatic change in the morphology of the layers visible in the WF maps reported later, due to the rippling of anodized layers.

The deconvolution into single chemically shifted components for the anodized layers is more difficult to achieve due to their broader features with respect to the pristine sample. To position the carbon in SiC components for the anodized spectra, the component at 283.8 eV of the pristine sample have been shifted by 0.16 eV and normalized according to the Si 2p lines. In the anodized layers the C in SiC component are about 15% larger in full width half maximum with respect to the pristine sample, which we attribute to the more complex interface between the substrate and the graphene layers after the anodization. We add to the anodized spectra, peaks for C sp^2 shifted to low BEs of 0.16 eV and larger of 15 % simulating a similar shift and broadening of the components of C in SiC. The sp^2 carbon peak in the anodized layers is related both to the multilayers and to the sp^2 patches of the single layer that are still intact after anodization. The buffer layer component has not been replicated in the anodized spectra because a Raman investigation [14] after the anodization has revealed that the buffer layer features from about 1200 to 1600 cm^{-1} are strongly suppressed after anodization. However, in order to prove the transformation of the buffer layer by photoemission, more accurate acquisitions are required, e.g. using low photon excitation energy or angle resolved acquisitions.

To complete the fit of the anodized layers a component at 286.5 eV has been added for the C-O bonds [37, 42] related to epoxy groups [23, 43], we can exclude the presence of C=O and COOH at higher BEs. The presence of a prevalent epoxy component is also confirmed by the O 1s BE at 532.3 eV [23] (Figure S5). The presence of epoxy groups on oxygen-treated graphitic material has been observed for atomic oxygen dosed under UHV conditions [23, 43], however it is uncommon to find such a good selection of the oxygen species for a sample treated by wet chemistry, for example the oxidation of HOPG to create graphene oxides leads to several functionalizations of oxygen including C=O and COOH [44]. This observation suggests that more oxidized species such as carbonyl and carboxyl groups are involved in the OER process [34]. The evidence for epoxy groups is also indicative of the fragmenting of the graphene layer due to the well-known oxidation mechanism which starts with the formation of chains of epoxy groups [45-47] that subsequently transform into C=O and break the continuity of the layer [48].

Interestingly, after anodization there are no signs of Si-O bonds in the Si 2p spectra, this remarkable observation underlines how the anodization happens only on the graphitic layers.

A further component at 284.2 eV has been added for the anodized sample. Because of its low BE it can be safely concluded that it is related to oxidized carbon, we therefore link it to amorphous carbon created by the anodization process. The loss of sp^2 structure can also be related to the OER reaction of heavily oxidized moieties to form O_2 and H_2O, the carbon radicals can recombine in several ways and also cause the fragmenting of the graphene structure.

3.3 PEEM and WF maps

To achieve a microscopic view of the samples, WF maps have been acquired by PEEM. The WF map of pristine EG is reported in Figure 4 along with two snapshots at different E-E_f values. Three different contrasts are detected in the WF map: the single layer, linear defective structures and multilayer graphene. The latter have been identified using the reflectance maps in Figure S3. From the WF histogram reported in Figure S6, the single layer graphene has a WF at 4.21 eV and occupies 67 % of the surface.
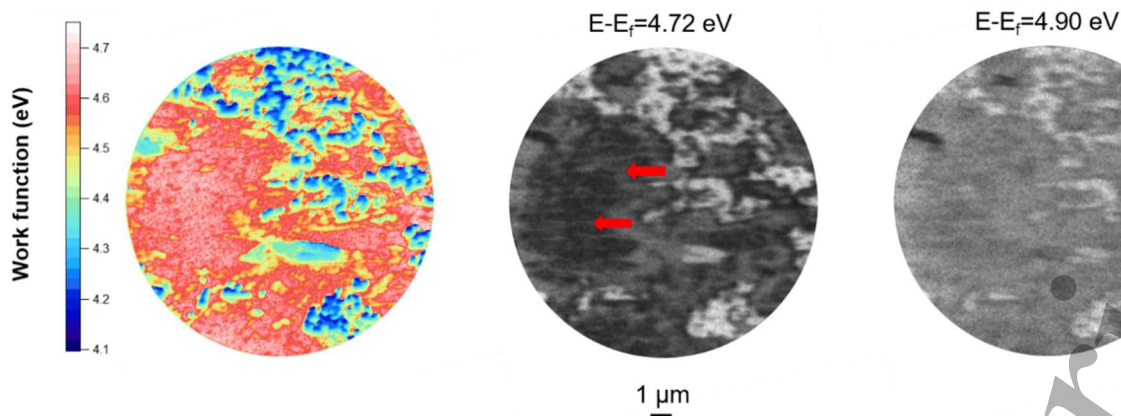
Figure 5. Anodized sample #1 PEEM analysis. On left the WF map, on the centre and right two snapshots acquired at E-E_f= 4.72 and 4.90 eV. The red arrows indicate the direction of oxygen redistribution.

The linear structures, probably due to the imperfections in the SiC crystal, have a more complex morphology and its WF peak in the histogram is broader with respect to the single layer, with its WF peak centred at 4.24 eV and occupying 31 % of the surface.

The multilayer regions at a higher WF of 4.31 eV occupy 2 % of the surface in very good agreement with Table 1. Analysing the single snapshot acquired close to the WF threshold, it is possible to distinguish the sample terraces at E-E_f=4.12 eV sometimes decorated with thin multilayer stripes, typical of EG on SiC Si-face [49]. Line profiles of the bottom part of image at E-E_f=4.12 eV reveal that the average width of the multilayer stripes is 90 nm, the minimum we measured was 70 nm. The multilayer stripes and terraces extend for several microns. The single layer graphene terraces range in size from 250 to 410 nm. These findings are consistent with previous investigations [50] even if comparisions are difficult because the dimensions of the terraces and multilayers are strongly dependent on the sample preparation. At E-E_f=4.90 eV it is possible to distinguish easily the large multilayers as darker areas.

After 30 seconds of anodization the WF map is very different, and PEEM results for the anodized sample #1 are reported in Figure 5. In Figure 5 the monolayer graphene can be distinguished in the snapshot at E-E_f=4.72 eV where the terrace lines are still visible. Line profiles acquired on the left part of the image confirm that these regions are about the same size as those observed in Figure 4. The contrast is inverted, the multilayers, are brighter, they are also large, on average 120 nm, and single layers appearing as, darker regions are wide, ranging from 290 to 520 nm. These features extend across roughly half of each image, or about 7 μm. The monolayer is strongly affected by the anodization, its WF varies from 4.2 eV for the pristine sample to about 4.7 eV. Using the methods employed in the previous sample it is also possible to see the large multilayers as dark areas in the snapshot at E-E_f=4.90 eV

and, interestingly, also bright areas are visible at this energy region which is different from EG (Figure 4).

The snapshots in Figure 5 help in interpreting the new morphology. In the snapshot at E-E_f=4.72 eV the bright features can be separated into bubble-like (white) and linear features (grey). The image at E-E_f=4.90 eV show the multilayer as darker areas and the bubble-like features are bright. Comparing these two images we can conclude that the bubble-like features are surrounded by the grey linear features. Notably it is recognisable that some of these features follow the direction of the terraces. The bubble-like features may be related to heavily oxidized species while the features that surround them, which have an intermediate WF (4.4-4.6 eV) from single layer (4.7 eV) and the bubble structures (4.2 eV), can be partially oxidized layers that are gradually transforming the single layer. Snapshots at a bigger field of view in Figure S7 confirm this hypothesis.

For the anodized sample #1 the oxidation of the single layer was incomplete because the morphology investigation by PEEM indicates patches similar to the pristine sample, especially for the single layer with visible terraces, the clear difference in WF for a single layer graphene can be linked to the oxidation of the buffer layer that consequently decoupled the graphene, and confirmed also by a previous Raman spectroscopy investigation [14].

For the anodized sample #2 a different WF landscape is revealed, as shown in Figure 6. It is immediately apparent that the surface experienced another transformation. The areas of single layers with terraces disappeared and a rough morphology is visible all over the surface. With a snapshot taken at different E-E_F two types of features are visible, small low WF particles and long linear features that occupy a greater part of the surface.

The remnants of the single layer zones are visible as the areas with WF of about 4.6 eV, but they are percolated by linear structures of intermediate WF of about ≈4.4 eV. Like anodized sample #1, at E-E_f =4.90 eV these are visible as faint dark areas which correspond to multilayers. Interestingly,
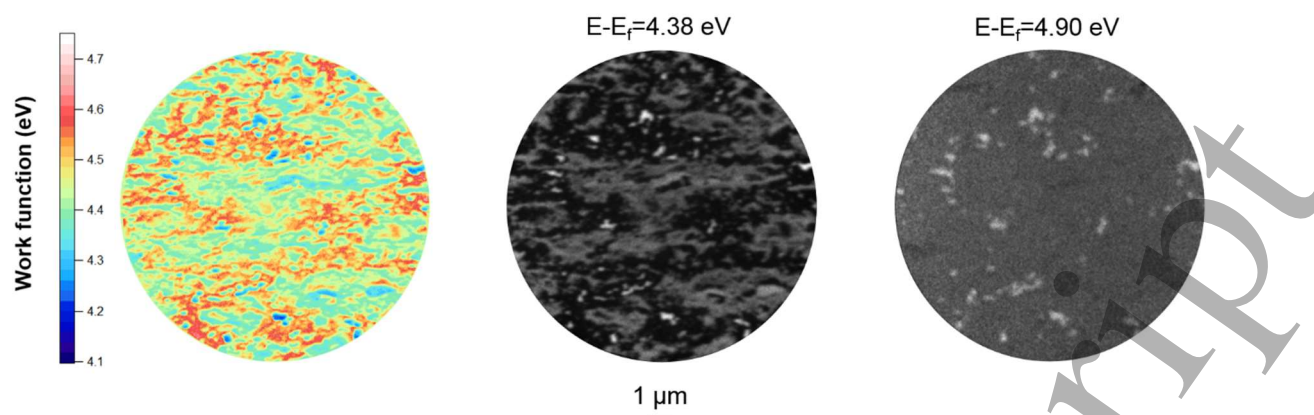
Figure 6. Anodized sample #2 PEEM analysis. On left the WF map, on the centre and right two snapshots acquired at $E-E_F$= 4.38 and 4.90 eV.

these areas are fuzzy on this image confirming that the multilayers' edges are functionalized with oxygen and they contribute to the increase in film capacitance, see discussion above in section 3.1.

Notably, the percolating structure is not completely isotropic, the features follow a direction, in this case horizontal, which is most probably the direction of the crystal terraces. This means that the anodization creates ripples following the substrate direction probably triggered by the increase defect density and dangling bonds on the surface due to the step edges. The ripples can be the result of water splitting and the creation of O_2 gas during the anodization.

Interestingly, the quantity of low WF bright spots decreased strongly from the anodized sample #1 and #2. Because they are surrounded by high WF regions ($\approx$4.6 eV), which we relate to previously pristine graphene, we think they are different from the bubble features of anodized sample #1. Indeed, from the analysis of Figure 5 and S7, the bubble features are considered the starting point of the anodization which spreads towards the single layer regions whereas after a long anodization time these features are surrounded by single layer graphene.

PEEM acquisition of anodized sample #2 shows strong differences in comparison with anodized sample #1, however the C 1s and O 1s photoemission lines are quite similar and the quantity of oxygen does not drastically increase with the anodization time. We attribute this apparent discrepancy of the two techniques to multistage transformation of the layer during the anodization process. As mentioned above in section 3.2, the Si 2p intensity reduction from the two anodized layers is due to substrate signal attenuation of three-dimensional features that dominated the surface of the anodized sample #2.

3.4 Anodization pathway hypothesis

In this paragraph we attempt to use our photoemission findings to rationalize the EG anodization route.

We hypothesize that in the first stage of the anodization the buffer layer and single layer graphene are oxidized mildly, O_2^-/OH^- species diffuse underneath EG and decouple the whole graphitic structure from the SiC substrate, as seen in the shift to low BEs in Figure 3. The buffer layer is expected to be the first to react because of its increased number of defects and dangling bonds [51], we expect an increase in reactivity especially in the vast regions where there are linear defective structures (Figure 4). We think that, on those linear structures, the anodization process creates bubble-like features (Figure 5), which we related to fragmented and heavily oxidized graphene. We also think that, these bubble-like features act as reservoir for oxygen for the anodization which expands towards the single layer regions exploiting the enhanced reactivity of the buffer layer and step edges [47], shown by arrows in Figure 5.

We also hypothesize a second stage of anodization, which still does not damage the substrate. In this step the diffusion of the oxygen moieties is complete and single layer graphene acquires ripples and is partially amorphized. Consequently, there is no up-take of oxygen but just a redistribution on the surface. We think that, the inability to oxidized the large multilayer graphene [14] can be understood by considering that the whole anodization process happens from the buffer and the single layer, leaving intact the large multilayer structures. However, after the anodization the multilayers images are fuzzier, see PEEM snapshot in Figure 6 with respect to the one in Figure 4. Indeed, fitting their edges with a sigmoid, we found that fitted full width at half maximum are about 140, 150 and 280 nm for Figure 4, Figure 5 and Figure 6, respectively. We link this decrease in sharpness to edge oxidation and therefore they contribute to the increase in the capacitance (see Table 1 and Figure S4). We think that smaller multilayer stripes at terrace edges can be oxidized because they are located in areas with an abundance of dangling bonds that are probably the preferred pathway for the redistribution of oxygen moieties. Finally, we link the micrometric rippling,

Author *et al*

easily visible in Figure 6, after long anodization times, to the formation of $O_2(g)$ and $H_2O(l)$ that lift the anodized graphene due to the OER.

4. Conclusion

In this work the anodization process for EG has been studied by XPS and PEEM. Several fundamental observations can be drawn from the experiments which elucidate the chemical and physical transformation that EG undergoes during the electrochemical treatment.

From the XPS, we think the main results are the decoupling of graphene by oxygen species [40, 41], which surprisingly do not react significantly with the SiC substrate, and the selective functionalization of the layer by epoxy groups. The detection of epoxy groups confirms the well-known fragmenting graphene process [45-47], while the absence of carbonyl and carboxyl species can be explained by their OER reaction with water to form O_2 [34]. Interestingly the amount of oxygen does not increase strongly with the anodization time, therefore we infer a diffusion and redistribution of oxygen moieties on the surface during the anodization.

The innovative PEEM acquisitions on electrochemical treated samples, allow one to understand the dramatic physical transformation of the layers during the anodization process. After only 30 seconds the sample is observed to be strongly modified by the process, with islands of graphene still visible along with bubble features that we relate to heavily oxidized parts. From the WF maps and PEEM images the pathway of oxygen diffusion on the surface from the oxidized fragments to the single layer regions are revealed.For long anodization times the layer becomes strongly rippled because of the O_2 evolution. The large regions of multilayer graphene are found to be only marginally involved in the anodization, their oxidized edges contribute to the increase in capacitance.

The combination of surface science techniques employed in this work has allowed us to make some speculation regarding the significant transformation that EG undergoes during the anodization. These results provide important information about graphitic materials for the OER showing that the layers are transformed due to the electrochemical conditions.

The degradation of EG due to OER illustrates both the anodization mechanism of graphene and the fundamental obstacle towards the implementation of electrolytic technologies based on anodic water splitting. The significant overpotential of OER accompanied with a degradation of graphene as a key aspect of all graphitic materials and motivates the use of catalysts both to protect graphite current collectors and reduce the electrical energy cost for sustainable hydrogen economy.

Acknowledgements

References

[1] Zhou X, Qiao J, Yang L and Zhang J 2014 A Review of Graphene-Based Nanostructural Materials for Both Catalyst Supports and Metal-Free Catalysts in PEM Fuel Cell Oxygen Reduction Reactions *Advanced Energy Materials* **4** 1301523.

[2] Hu H, Xin J H, Hu H, Wang X and Kong Y 2015 Metal-free graphene-based catalyst—Insight into the catalytic activity: A short review *Applied Catalysis A: General* **492** 1-9.

[3] Li Y, Zhou W, Wang H, Xie L, Liang Y, Wei F, Idrobo J-C, Pennycook S J and Dai H 2012 An oxygen reduction electrocatalyst based on carbon nanotube–graphene complexes *Nature Nanotechnology* **7** 394-400.

[4] Jahan M, Liu Z and Loh Kian P 2013 A Graphene Oxide and Copper-Centered Metal Organic Framework Composite as a Tri-Functional Catalyst for HER, OER, and ORR *Advanced Functional Materials* **23** 5363-5372.

[5] Allen M J, Tung V C and Kaner R B 2010 Honeycomb Carbon: A Review of Graphene *Chemical Reviews* **110** 132-145.

[6] Chen D, Tang L and Li J 2010 Graphene-based materials in electrochemistry *Chem Soc Rev* **39** 3157-3180.

[7] Bai H, Li C and Shi G 2011 Functional Composite Materials Based on Chemically Converted Graphene *Advanced Materials* **23** 1089-1115.

[8] Agnoli S and Favaro M 2016 Doping graphene with boron: a review of synthesis methods, physicochemical characterization, and emerging applications *Journal of Materials Chemistry A* **4** 5002-5025.

[9] Wang H, Maiyalagan T and Wang X 2012 Review on Recent Progress in Nitrogen-Doped Graphene: Synthesis, Characterization, and Its Potential Applications *ACS Catalysis* **2** 781-794.

[10] Soldano C, Mahmood A and Dujardin E 2010 Production, properties and potential of graphene *Carbon* **48** 2127-2150.

[11] Janas D and Koziol K K 2014 A review of production methods of carbon nanotube and graphene thin films for electrothermal applications *Nanoscale* **6** 3037-3045.

[12] Riedl C, Coletti C and Starke U 2010 Structural and electronic properties of epitaxial graphene on SiC(0 0 0 1): a review of growth, characterization, transfer doping and hydrogen intercalation *Journal of Physics D: Applied Physics* **43**

[13] Emtsev K V, Bostwick A, Horn K, Jobst J, Kellogg G L, Ley L, McChesney J L, Ohta T, Reshanov S A, Röhrl J, Rotenberg E, Schmid A K, Waldmann D, Weber H B and Seyller T 2009 Towards wafer-size graphene layers by atmospheric pressure graphitization of silicon carbide *Nature Materials* **8** 203-207.

[14] Vagin M Y, Sekretaryova A N, Ivanov I G, Håkansson A, Iakimov T, Syväjärvi M, Yakimova R, Lundström I and Eriksson M 2017 Monitoring of epitaxial graphene anodization *Electrochimica Acta* **238** 91-98.

[15] Ang P K, Chen W, Wee A T S and Loh K P 2008 Solution-Gated Epitaxial Graphene as pH Sensor *Journal of the American Chemical Society* **130** 14392-14393.

[16]   Chen D, Feng H and Li J 2012 Graphene Oxide: Preparation, Functionalization, and Electrochemical Applications *Chemical Reviews* **112** 6027-6053.

[17]   An K H, Kim W S, Park Y S, Moon J M, Bae D J, Lim S C, Lee Y S and Lee Y H 2001 Electrochemical Properties of High-Power Supercapacitors Using Single-Walled Carbon Nanotube Electrodes *Advanced Functional Materials* **11** 387-392.

[18]   Chabot V, Higgins D, Yu A, Xiao X, Chen Z and Zhang J 2014 A review of graphene and graphene oxide sponge: material synthesis and applications to energy and the environment *Energy & Environmental Science* **7**

[19]   Chen S, Duan J, Jaroniec M and Qiao S Z 2014 Nitrogen and Oxygen Dual-Doped Carbon Hydrogel Film as a Substrate-Free Electrode for Highly Efficient Oxygen Evolution Reaction *Advanced Materials* **26** 2925-2930.

[20]   Ma Tian Y, Dai S, Jaroniec M and Qiao Shi Z 2014 Graphitic Carbon Nitride Nanosheet–Carbon Nanotube Three-Dimensional Porous Composites as High-Performance Oxygen Evolution Electrocatalysts *Angewandte Chemie International Edition* **53** 7281-7285.

[21]   Favaro M, Ferrighi L, Fazio G, Colazzo L, Di Valentin C, Durante C, Sedona F, Gennaro A, Agnoli S and Granozzi G 2015 Single and Multiple Doping in Graphene Quantum Dots: Unraveling the Origin of Selectivity in the Oxygen Reduction Reaction *ACS Catalysis* **5** 129-144.

[22]   Hossain M Z, Razak M B A, Yoshimoto S, Mukai K, Koitaya T, Yoshinobu J, Sone H, Hosaka S and Hersam M C 2014 Aqueous-Phase Oxidation of Epitaxial Graphene on the Silicon Face of SiC(0001) *The Journal of Physical Chemistry C* **118** 1014-1020.

[23]   Barinov A, Malcioğlu O B, Fabris S, Sun T, Gregoratti L, Dalmiglio M and Kiskinova M 2009 Initial Stages of Oxidation on Graphitic Surfaces: Photoemission Study and Density Functional Theory Calculations *The Journal of Physical Chemistry C* **113** 9009-9013.

[24]   Favaro M, Perini L, Agnoli S, Durante C, Granozzi G and Gennaro A 2013 Electrochemical behavior of N and Ar implanted highly oriented pyrolytic graphite substrates and activity toward oxygen reduction reaction *Electrochimica Acta* **88** 477-487.

[25]   Liang Y, Li Y, Wang H, Zhou J, Wang J, Regier T and Dai H 2011 Co3O4 nanocrystals on graphene as a synergistic catalyst for oxygen reduction reaction *Nature Materials* **10** 780-786.

[26]   Liang Y, Wang H, Zhou J, Li Y, Wang J, Regier T and Dai H 2012 Covalent Hybrid of Spinel Manganese–Cobalt Oxide and Graphene as Advanced Oxygen Reduction Electrocatalysts *Journal of the American Chemical Society* **134** 3517-3523.

[27]   Toghan A, Rösken L M and Imbihl R 2010 The Electrochemical Promotion of Ethylene Oxidation at a Pt/YSZ Catalyst *Chem. Phys. Chem.* **11** 1452-1459.

[28]   Luerßen B, Mutoro E, Fischer H, Günther S, Imbihl R and Janek J 2006 In Situ Imaging of Electrochemically Induced Oxygen Spillover on Pt/YSZ Catalysts *Angew. Chem.* **45** 1473-1476.

[29]   Janek J, Luerßen B, Mutoro E, Fischer H and Günther S 2007 In situ imaging of electrode processes on solid electrolytes by photoelectron microscopy and microspectroscopy – the role of the three-phase boundary *Top. Catal.* **44** 399-407.

[30]   Burnett T, Yakimova R and Kazakova O 2011 Mapping of local electrical properties in epitaxial graphene using electrostatic force microscopy *Nano Lett* **11** 2324-2328.

[31]   Ivanov I G, Hassan J U, Iakimov T, Zakharov A A, Yakimova R and Janzén E 2014 Layer-number determination in graphene on SiC by reflectance mapping *Carbon* **77** 492-500.

[32]   Mathieu C, Barrett N, Rault J, Mi Y Y, Zhang B, de Heer W A, Berger C, Conrad E H and Renault O 2011 Microscopic correlation between chemical and electronic states in epitaxial graphene on SiC(0001) *Physical Review B* **83** 235436.

[33]   Lim C X, Hoh H Y, Ang P K and Loh K P 2010 Direct Voltammetric Detection of DNA and pH Sensing on Epitaxial Graphene: An Insight into the Role of Oxygenated Defects *Analytical Chemistry* **82** 7387-7393.

[34]   Suen N-T, Hung S-F, Quan Q, Zhang N, Xu Y-J and Chen H M 2017 Electrocatalysis for the oxygen evolution reaction: recent development and future perspectives *Chemical Society Reviews* **46** 337-365.

[35]   Shinagawa T, Garcia-Esparza A T and Takanabe K 2015 Insight on Tafel slopes from a microkinetic analysis of aqueous electrocatalysis for energy conversion *Scientific Reports* **5** 13801.

[36]   Yang D, Velamakanni A, Bozoklu G, Park S, Stoller M, Piner R D, Stankovich S, Jung I, Field D A, Ventrice C A and Ruoff R S 2009 Chemical analysis of graphene oxide films after heat and chemical treatments by X-ray photoelectron and Micro-Raman spectroscopy *Carbon* **47** 145-152.

[37]   Ganguly A, Sharma S, Papakonstantinou P and Hamilton J 2011 Probing the Thermal Deoxygenation of Graphene Oxide Using High-Resolution In Situ X-ray-Based Spectroscopies *The Journal of Physical Chemistry C* **115** 17009-17019.

[38]   Ouerghi A, Silly M G, Marangolo M, Mathieu C, Eddrief M, Picher M, Sirotti F, El Moussaoui S and Belkhou R 2012 Large-Area and High-Quality Epitaxial Graphene on Off-Axis SiC Wafers *ACS Nano* **6** 6075-6082.

[39]   Pallecchi E, Lafont F, Cavaliere V, Schopfer F, Mailly D, Poirier W and Ouerghi A 2014 High Electron Mobility in Epitaxial Graphene on 4H-SiC(0001) via post-growth annealing under hydrogen *Scientific Reports* **4** 4558.

[40]   Ostler M, Fromm F, Koch R J, Wehrfritz P, Speck F, Vita H, Böttcher S, Horn K and Seyller T 2014 Buffer layer free graphene on SiC(0001) via interface oxidation in water vapor *Carbon* **70** 258-265.

[41]   Oida S, McFeely F R, Hannon J B, Tromp R M, Copel M, Chen Z, Sun Y, Farmer D B and Yurkas J 2010 Decoupling graphene from SiC(0001) via oxidation *Physical Review B* **82** 041411(R).

[42]   Carraro F, Calvillo L, Cattelan M, Favaro M, Righetto M, Nappini S, Píš I, Celorrio V, Fermín D J, Martucci A, Agnoli S and Granozzi G 2015 Fast One-Pot Synthesis of MoS2/Crumpled Graphene p–n Nanonjunctions for Enhanced Photoelectrochemical Hydrogen Production *ACS Applied Materials & Interfaces* **7** 25685-25692.

[43]   Hossain M Z, Johns J E, Bevan K H, Karmel H J, Liang Y T, Yoshimoto S, Mukai K, Koitaya T, Yoshinobu J, Kawai M, Lear A M, Kesmodel L L, Tait S L and Hersam M C 2012 Chemically homogeneous and thermally reversible oxidation of epitaxial graphene *Nature Chemistry* **4** 305-309.

Author *et al*

[44]   Favaro M, Agnoli S, Cattelan M, Moretto A, Durante C, Leonardi S, Kunze-Liebhäuser J, Schneider O, Gennaro A and Granozzi G 2014 Shaping graphene oxide by electrochemistry: From foams to self-assembled molecular materials *Carbon* **77** 405-415.

[45]   Fujii S and Enoki T 2010 Cutting of Oxidized Graphene into Nanosized Pieces *Journal of the American Chemical Society* **132** 10034-10041.

[46]   Sk M A, Huang L, Chen P and Lim K H 2016 Controlling armchair and zigzag edges in oxidative cutting of graphene *Journal of Materials Chemistry C* **4** 6539-6545.

[47]   Li J L, Kudin K N, McAllister M J, Prud'homme R K, Aksay I A and Car R 2006 Oxygen-driven unzipping of graphitic materials *Phys Rev Lett* **96** 176101.

[48]   Li Z, Zhang W, Luo Y, Yang J and Hou J G 2009 How Graphene Is Cut upon Oxidation? *Journal of the American Chemical Society* **131** 6320-6321.

[49]   Hass J, de Heer W A and Conrad E H 2008 The growth and morphology of epitaxial multilayer graphene *Journal of Physics: Condensed Matter* **20**

[50]   Man K L and Altman M S 2012 Low energy electron microscopy and photoemission electron microscopy investigation of graphene *J. Phys. Condens. Matter.* **24** 314209.

[51]   Ristein J, Mammadov S and Seyller T 2012 Origin of doping in quasi-free-standing graphene on silicon carbide *Phys Rev Lett* **108** 246104.